Chemical Geology 547 (2020) 119669

Contents lists available at ScienceDirect

Chemical Geology

journal homepage: www.elsevier.com/locate/chemgeo

Effects of divalent heavy metal cations on the synthesis and characteristics of magnetite

Huihui Huang[a,b], Jin Wang[c,d], Ruining Yao[a], Benjamin C. Bostick[e], Henning Prommer[f,g], Xiaodong Liu[a,*], Jing Sun[b,f,g,**]

[a] Institute of Polar Environment & Anhui Key Laboratory of Polar Environment and Global Change, School of Earth and Space Sciences, University of Science and Technology of China, Hefei, Anhui 230026, China
[b] State Key Laboratory of Environmental Geochemistry, Institute of Geochemistry, Chinese Academy of Sciences, Guiyang 550081, China
[c] School of Environmental Science and Engineering, Guangzhou University, Guangzhou 510006, China
[d] Guangdong Provincial Key Laboratory of Radionuclides Pollution Control and Resources, Guangzhou 510006, China
[e] Lamont-Doherty Earth Observatory, PO Box 1000, 61 Route 9W, Palisades, NY 10964, United States
[f] School of Earth Sciences, University of Western Australia, 35 Stirling Hwy, Perth, WA 6009, Australia
[g] CSIRO Land and Water, Private Bag No. 5, Wembley, WA 6913, Australia

ARTICLE INFO

Editor: Karen Johannesson

Keywords:
Iron
Magnetite
Heavy metal
Mineralogy
Co-precipitation
Adsorption

ABSTRACT

Despite decades-long research efforts, the remediation of groundwater contaminated by heavy metals has remained a significant challenge. Recent studies have demonstrated that in situ formation of magnetite might be an effective method to more permanently immobilize metal(loid)s. However, how the co-existence of additional heavy metals affects the synthesis of magnetite under environmentally relevant conditions and how it affects the associated heavy metal removal efficiency have remained unclear. Here, a common magnetite synthesis procedure was used to synthesize Cu-, Cd-, and Pb-substituted magnetites at circumneutral pH with variable heavy metal concentrations. The synthesized mineral products were then subjected to digestion, Mössbauer, XRD, SEM-EDS, magnetic susceptibility and surface area measurements, as well as isothermal adsorption experiments. The presence of additional divalent heavy metals during synthesis affected the characteristics of the Fe mineral products. Magnetite formed in the presence of heavy metals was poorly crystalline and impure. The mineralogy and morphology of the products was regulated by the surface affinity of the heavy metal. The co-existence of divalent heavy metal cations that have higher surface affinity than Fe(II) suppressed the mineral growth of more crystalline Fe oxides, including magnetite. Minerals synthesized in the absence of heavy metals had higher capacity and affinity for heavy metals than minerals synthesized in the presence of those metals because of the effects of altered mineral surface structure and surface area on adsorption. These results help us understand how different types and concentrations of heavy metals affect magnetite synthesis and its suitability for in situ groundwater remediation.

1. Introduction

Groundwater contamination is pervasive. It is threatening drinking water resources and other receptors around the world. Among different types of contaminants, toxic heavy metals are particularly difficult to mitigate (Liu et al., 2019; Wang et al., 2020a,b). Unlike a wide range of organic pollutants, inorganic metals cannot be degraded (Adriano et al., 2004). An ideal mitigation strategy for heavy metal contamination would therefore aim to completely remove all contaminated soils/sediments and groundwater from the polluted site. A complete physical removal, however, is often impractical and too costly due to the sheer volume of sediments involved. To minimize the risks of metal release and off-site transport, routinely applied mitigation strategies often focus on plume containment or aquifer restoration, with the ultimate objective of decreasing the metal concentrations in groundwater (Liu et al., 2016; Statham et al., 2016). Although this seems a straightforward objective, in practice it is difficult to accomplish. Given traditional methods such as pump-and-treat are often unable to remediate

* Corresponding author.
** Correspondence to: J. Sun, State Key Laboratory of Environmental Geochemistry, Institute of Geochemistry, Chinese Academy of Sciences, Guiyang 550081, China.
E-mail addresses: ycx@ustc.edu.cn (X. Liu), sunjing@mail.gyig.ac.cn (J. Sun).

https://doi.org/10.1016/j.chemgeo.2020.119669
Received 21 February 2020; Received in revised form 8 May 2020; Accepted 12 May 2020
Available online 16 May 2020

groundwater heavy metal contamination in a timely and cost effective manner, it has become increasingly popular to aim for a significant contaminant mitigation by immobilizing metals onto or within mineral phases in situ (EPA, 2013; Fu et al., 2015).

The effectiveness and the longevity of the employed in situ immobilization technique both rely on producing minerals that successfully retain heavy metals while also remaining stable under the aquifer's native geochemical conditions. To date, heavy metal immobilization mostly involves the use of soluble or mineral-form amendments. For example, zero-valent iron (ZVI) methods have been used extensively within permeable reactive barriers (PRBs) to intercept contaminant plumes (Noubactep et al., 2012). Unfortunately, PRB-based methods are often troubled by successively decreasing barrier permeabilities that result from the production of voluminous corrosion products, ZVI surface passivation and incomplete adsorption (Crane and Scott, 2012; Noubactep et al., 2012). Alternatively, soluble oxidants such as permanganate may also be amended to the groundwater, targeted at oxidizing Fe(II) and thereby forming Fe(III) (oxyhydr)oxides in situ, which have a well-known high affinity for heavy metals (Sorlini and Gialdini, 2010). Such methods, however, are problematic in that the neoformed minerals often become unstable when the aquifer returns to native anaerobic condition, therefore re-contaminating the groundwater.

To eliminate the latter problem, recent studies suggested that magnetite can co-precipitate arsenic (As) into its crystal structure during formation and, once formed, magnetite can also act an effective sorbent, capable of retaining additional advected As (e.g., Coker et al., 2006; Sun et al., 2016a; Sun et al., 2016b; Sun et al., 2018b). Besides As metalloid oxyanions, various other studies showed that magnetite can also retain a wide range of heavy metal cations through co-precipitation (e.g., Cr^{3+}, Co^{2+}, Ni^{2+}, Cu^{2+}, Zn^{2+} and Cd^{2+}) (e.g., Cooper et al., 2000; Muehe et al., 2013; Schwertmann and Cornell, 2008) and/or surface adsorption (e.g., Ni^{2+}, Cu^{2+}, Zn^{2+}, Ni^{2+} and Pb^{2+}) (e.g., Ge et al., 2012; Nassar, 2010). Compared to many common Fe minerals, magnetite is distinctly more thermodynamically stable under the suboxic to anoxic conditions that are characteristic of most heavy metal contaminated aquifers (Delemos et al., 2006; Sun et al., 2016b). In situ magnetite formation can, therefore, potentially provide a long-term remedial option for heavy metal contaminated groundwater. However, to date, it remains largely unclear how different types and concentrations of heavy metal ions would affect magnetite synthesis and its effectiveness during groundwater in situ remediation.

The main objectives of this study therefore were (i) to examine the effects of different heavy metals on the mineralogy and morphology of the product of a common magnetite synthesis procedure; (ii) to quantify heavy metal substitution within the mineral structure under different initial concentrations; and (iii) to compare the sorption capacity of the mineral product with and without heavy metal substitution. Co-precipitation of ferrous and ferric Fe with a molar ratio of 1:2 was used for magnetite synthesis in this study. Divalent heavy metals including Cu, Cd and Pb (collectively Me^{2+}) were individually added during synthesis with two different Fe:Me molar ratios of 10:1 and 100:1. The mineral products were characterized using a number of mineralogical techniques. The magnitude of metal substitution was determined by digestion. Sorption capacity for heavy metals on the mineral product was quantified using isotherms at mildly acidic pH. Control experiments without additional heavy metal cations (other than Fe) were also conducted and analyzed in parallel for comparison.

2. Methods and materials

2.1. Mineral synthesis procedure

In this study, the Fe mineral magnetite was synthesized in an O_2-free glove box (N_2 > 99.9995%) by co-precipitating ferrous and ferric Fe from a ferrous sulfate and a ferric sulfate mixed solution with a Fe (II):Fe(III) ratio of 1:2 at pH 6.5–7. This procedure is commonly used for magnetite synthesis in alkaline (pH > 8) systems (Faiyas et al., 2010; Jolivet et al., 2004; Schwertmann and Cornell, 2008), but its efficacy is not well studied at circumneutral pH that more closely mimics typical aquifer conditions. All solutions were prepared freshly by dissolving the reagents in O_2-free deionized (DI) water (purged with high purity N_2) in centrifuge tubes. The solution initially contained 66.7 mM $FeSO_4$ and 66.7 mM $Fe_2(SO_4)_3$ and was acidic. The mineral precipitation was then initiated by raising the pH to 7 by adding a NaOH (5 M) solution. During synthesis, the solution was mixed thoroughly with a glass rod, while the pH was measured every 5 min using a calibrated pH meter and (re)adjusted to pH 7. Once the measured pH values remained stable over three subsequent measurements, the sample was sealed and aged for 24 h in the glove box. To investigate the effects of metal ion additions on mineral synthesis, eight additional experiments were conducted simultaneously as described above but each with an additional metal cation (Me) or a different concentration of the amended metal. Four metals including Me = Na, Cu, Cd and Pb, and two concentrations including 2 and 20 mM, i.e., Fe:Me molar ratios of 100:1 and 10:1 were tested in this study. Because $PbCl_2$ and $PbSO_4$ are hard to dissolve, whereas $Pb(NO_3)_2$ is soluble, Pb was added as $Pb(NO_3)_2$. The other metals (i.e., Na, Cu, and Cd) were then also added as nitrate-based chemicals for comparison purpose. All chemicals used in this study were of analytical grade. The initial ionic strength of the solutions was approximately 0.62 ± 0.03 M depending on metal ion additions.

After the 24 h-long aging period, the sealed centrifuge tubes were taken out of the glove box and the mineral precipitates were separated from the supernatant through centrifugation at 9000 rpm (9060 *g*) for 10 min. The supernatant was filtered to 0.22 μm using Nylon syringe filters (Whatman) in the glove box, and acidified to 1% HCl. The concentrations of metal ions in the supernatant were determined by inductively coupled plasma optical emission spectrometry (PerkinElmer Optima 7300DV ICP-OES) following a previously published procedure (Sun et al., 2016c). Based on the analysis of reference materials, the analytical uncertainty of the used ICP-OES machine was estimated to be <1% of the measured concentrations. The yields of Fe oxides were calculated based on the differences between the amounts of Fe added and the contents of Fe in the supernatants after synthesis. The obtained mineral precipitates were subsampled. For each sample, a part of the mineral precipitates was washed with N_2-purged 0.06 M HCl (pH < 2) to remove amorphous metal hydroxides and adsorbed cations, before being rinsed with N_2-purged DI water until free of electrolytes. The treated sample was then immersed in ethanol (≥99.7%), and magnetic particles were separated by a magnet. The acid wash, DI water wash and magnetic separation steps together are referred to hereafter as isolation, and the isolated samples are referred to hereafter as crystalline products. The rest of the mineral precipitates were simply rinsed with N_2-purged DI water and used as the fresh (unisolated) products for comparison. Other than centrifugation, the steps were all conducted in the glove box. The fresh and crystalline mineral products were then dried using a vacuum freeze dryer and stored in an O_2-free environment until further analysis.

2.2. Compositional and mineralogical analyses of the mineral precipitates

The mineral precipitates were characterized by a number of different techniques for their composition, morphology and structure (Table S1). To quantify the elemental composition, the fresh and crystalline mineral precipitates were digested following the procedure in Schwertmann and Cornell (2008). The digestions were conducted with 50 mg of freeze-dried solid samples and 5 mL of 6 M HCl in glass digestion tubes. They were heated to 60 °C in a water bath on a hot plate for 30 min. Once completed and cooled to room temperature, 1 mL of the digestate was transferred to a 10 mL colorimetric tube and diluted with 5% HCl. Dissolved concentrations of metal ions were determined by ICP-OES as described above. Laboratory synthesized and commercially obtained pure ferrihydrite, goethite and magnetite were

Table 1
Characteristics of the fresh and crystalline Fe mineral products synthesized in this study.

Synthesis condition	*Fe:Me molar ratio*		*Magnetic susceptibility (m^3 kg^{-1})*		*Specific surface area (m^2 g^{-1})*	
	Fresh	*Crystalline*	*Fresh*	*Crystalline*	*Fresh*	*Crystalline*
Fe Only	–	–	*5674 ± 19*	*4883 ± 2*	*108.8 ± 0.4*	*96.2 ± 0.7*
Fe:Na = 100:1	–	–	*4696 ± 12*	*4648 ± 2*	*128.2 ± 0.4*	*106.9 ± 0.5*
Fe:Na = 10:1	–	–	*4792 ± 17*	*4342 ± 2*	*135.2 ± 0.5*	*99.7 ± 0.3*
Fe:Cu = 100:1	*132 ± 9*	*770 ± 40*	*3631 ± 4*	*2447 ± 2*	*147.3 ± 0.9*	*119.6 ± 0.4*
Fe:Cu = 10:1	*13.4 ± 0.7*	*64 ± 10*	*236 ± 2*	*389 ± 1*	*184.6 ± 0.9*	*192.8 ± 1.2*
Fe:Cd = 100:1	*295 ± 15*	*360 ± 18*	*3270 ± 6*	*3771 ± 2*	*133.4 ± 0.4*	*119.6 ± 0.6*
Fe:Cd = 10:1	*67 ± 5*	*85 ± 6*	*3798 ± 2*	*5172 ± 4*	*163.2 ± 0.7*	*137.3 ± 0.3*
Fe:Pb = 100:1	*149 ± 10*	*676 ± 56*	*840 ± 5*	*646 ± 1*	*120.3 ± 0.2*	*117.9 ± 0.4*
Fe:Pb = 10:1	*16.4 ± 1.9*	–[a]	*46 ± 1*	–[a]	*176.2 ± 0.5*	–[a]

Note:
[a] No crystalline sample existed for Fe:Pb = 10:1 condition, as the synthesized minerals dissolved completely in the acid wash step during isolation.

simultaneously digested and analyzed. Based on the results obtained for the known minerals, the recovery rate of the digestion method showed to be within 100 ± 5%.

To examine the effect of heavy metal addition on Fe mineralogy, the fresh mineral precipitates were characterized by powder X-ray diffraction (XRD) and ^{57}Fe Mössbauer spectroscopy. XRD analysis was carried out using a model TTR-III diffractometer, with a Cu Kα radiation source (λ = 1.5406 Å) at 20–60 kV and 10–300 mA. Each of the samples was front-loaded into a cavity of an XRD sample holder and scanned over 2-Theta range from 3° to 80°, with a step size of 0.02° and a counting time of 3 s per step. The diffraction patterns were matched against the standard 2–2004 PDF database using MDI Jade 6.5. ^{57}Fe Mössbauer spectra were obtained using an OXEORDMS-500 constant acceleration spectrometer in transmissive geometry. A ^{57}Co source embedded in a Rh matrix was used at room temperature. Velocity (gamma-ray energy) was calibrated using a 25 μm α-Fe foil, and the isomer shift (I.S.) values were given relative to the center of α-Fe at 298 K. The Mössbauer spectra fitting routine was consistent with previously published procedures using MossWinn (Klencsar et al., 1996).

Highly magnified images and high-resolution compositional analysis of the fresh and crystalline mineral precipitates were obtained using scanning electron microscope (SEM) and energy dispersive spectroscopy (EDS). SEM-EDS analysis was conducted with a GeminiSEM 500 (ZEISS, Germany) field emission scanning electron micro-analyzer equipped with an EDS detector (Aztec, Oxford). The micro-analyzer was operated at an accelerating voltage of 20 kV, and the beam was defocused to 0.1–2 μm. Additionally, magnetic susceptibility (MS) and specific surface area (SSA) of the fresh and crystalline mineral precipitates were determined. MS, which is overwhelmingly sensitive to the presence of magnetite, was measured with a Bartington MS2 portable susceptibility meter. For SSA measurement, the samples were degassed for 30 min at 100 °C under vacuum and then analyzed with a Micromeritics ASAP 2460 by a 9-point Brunauer–Emmett–Teller (BET) isotherm using N_2 as adsorbate.

2.3. Adsorption isotherms

The adsorption capacity of the crystalline mineral precipitates for heavy metals was determined based on adsorption isotherms. Duplicate isotherm experiments were conducted in a glove box and all the solutions were purged with N_2 before use. To perform isotherm experiments, solutions containing up to 8 mM Cu, 8 mM Cd or 1.8 mM Pb were prepared. The metal ions were added from freshly prepared Cu$(NO_3)_2$, Cd$(NO_3)_2$ and Pb$(NO_3)_2$ stock solutions, respectively. All the isotherm experiments were performed with a background electrolyte of 50 mM $NaNO_3$. To prevent heavy metal ions from forming hydroxide precipitates in the solution, similar to many literature adsorption experiments with these heavy metals (Table S2), the adsorption isotherm experiment in this study was performed under mildly acidic condition, i.e., at pH 5.6. The pH of each solution was buffered with 10 mM of 2-(N-morpholino)ethanesulfonic acid (MES) and adjusted to pH 5.6 with 0.1 M NaOH. After pH adjustment, the solutions were subsampled for determining initial dissolved metal concentrations. Freeze-dried mineral precipitates were then added to the solutions, with a solid density of 1 g L^{-1}. The suspensions were equilibrated at room temperature for 24 h, and then filtered to 0.22 μm. They were compared to mineral-free controls to differentiate between adsorption and potential mineral precipitation or retention by the container walls or filters. Dissolved concentrations of heavy metal ions in the initial solutions and in the filtrates were measured by ICP-OES as described above. The sorbed concentrations were taken to be the differences between dissolved metal concentrations in the initial solutions and the corresponding filtrates at the end of the experiment.

3. Results

3.1. Composition of the mineral products

Based on mass balance calculation using dissolved Fe concentrations in the initial solution and the supernatant after mineral synthesis, ~90% of the added Fe precipitated under Fe only condition (Table S3). The identity and concentration of the added metal ions (i.e., Na, Cu, Cd and Pb) did not change the yield of Fe precipitates, although the quantity of divalent heavy metal incorporated into the mineral products was variable. Copper and Pb were strongly retained (~99%) in the precipitates at Fe:Me ratios of 10 and 100, while only 51 ± 14% of the added Cd was removed under the same conditions (Table S3).

The mineral products synthesized in the presence of Cu were partially resistant to the acid wash step (0.06 M HCl) during isolation. This isolation step increased the Fe:Cu ratio from 132 and 13.4, slightly higher than their initial ratios, to 770 and 64 (Table 1). This 5–6 fold increase in the Fe:Cu ratio indicates that much of the Cu that precipitated was associated with amorphous phases or adsorbed on the Fe mineral products, because those pools are effectively extracted by HCl. Compared with Cu, Cd was incorporated less efficiently but more permanently. The Fe:Cd ratios were 300 and 70 in the fresh mineral precipitates, respectively, and did not change significantly in the isolated, crystalline products. This implies that most of the Cd was associated with more crystalline mineral phases (Table 1). The behavior of Pb varied more with the initial Fe:Pb ratio. When the Fe:Pb ratio was 100 (lower Pb additions in solution), the Fe:Pb ratio was 149 in the fresh mineral precipitates, and increased by ~4.5 times after isolation (Table 1). At lower Fe:Pb ratios (higher Pb additions), the Fe:Pb ratio of the fresh mineral precipitates was 18.3. However, the resulting minerals completely dissolved during the acid extraction step. Therefore, much of the Pb appears to be bound in amorphous minerals, and higher additions of Pb resulted in most of the precipitates being amorphous.

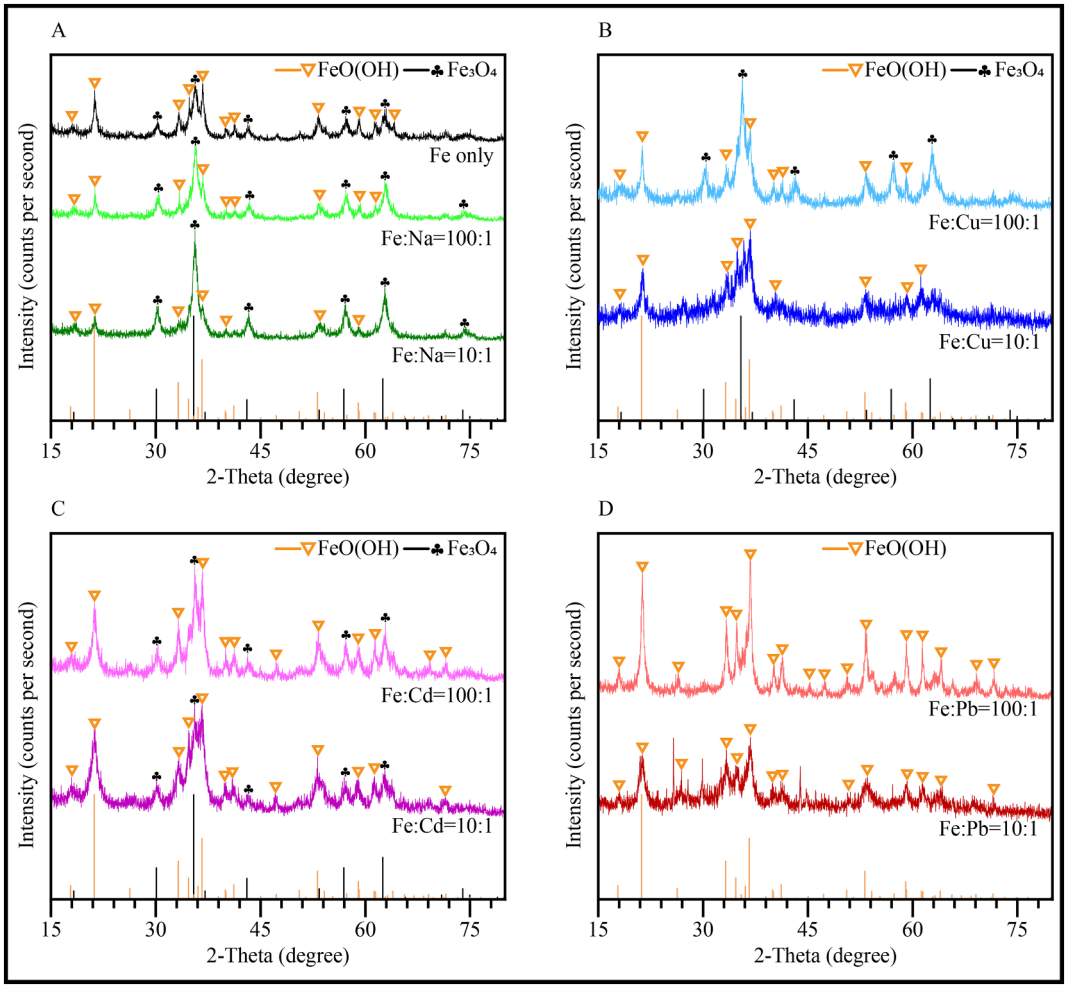

Fig. 1. XRD patterns of the fresh Fe mineral products synthesized under (A) Fe only and Na-, (B) Cu-, (C) Cd- and (D) Pb-bearing conditions. The molar ratios of Fe ions to other metal ions are shown in the figure. The spectra are vertically offset for clarity. XRD patterns of magnetite (Fe_3O_4, JCPDS no. 00-19-0629) and goethite (FeO(OH), JCPDS no. 01–081-0463) mineral references are included for comparison.

3.2. Mineralogical and morphological characteristics of the products

Magnetite and goethite phases were identified by XRD in the fresh mineral precipitates synthesized under Fe only condition and Na-bearing conditions (Fig. 1A). Owing to the presence of magnetite, the magnetic susceptibility (MS) of these mineral precipitates was ~5000 $m^3\ kg^{-1}$ (Table 1), a value typical of micro- to nanocrystalline magnetite (Maher, 1988). The MS remained high even after isolation, indicating the synthesized magnetite resisted the acid wash. The XRD spectra of the fresh mineral precipitates under low-Cu and low- and high-Cd conditions were similar to those of the Fe only conditions. The MS of these minerals was lower than the MS of the minerals under Fe only conditions, but still higher than 3000 $m^3\ kg^{-1}$. Under high-Cu conditions and low- and high-Pb conditions, only goethite was detected based on XRD, while magnetite diffraction peaks disappeared (Fig. 1). Accordingly, the MS of these minerals was low. Furthermore, for all of the samples, their XRD diffraction lines exhibited a line broadening effect typical of nanoparticles. Consistent with fine particle sizes, all the samples had a high SSA of 100–200 $m^2\ g^{-1}$ (Table 1). Especially for the minerals synthesized under high concentrations of additional heavy metals, their XRD peaks were even broader and their SSAs were even higher. Based on the Scherrer equation (Scherrer, 1918) using full width at half maximum (FWHM) values of the main XRD diffraction peaks, including (220), (311), (440), (511) facets of goethite and (110), (111), (130), (221) facets of magnetite, the particle sizes of the synthesized goethite and magnetite were estimated to be 10–22 and 13–15 nm, respectively (Table S4). Quartz, which is highly crystalline, had a FWHM of < 0.1° on the same diffractometer, confirming that the calculated mineral width was not an artifact induced by instrumental broadening. XRD peak shift can be indicative of structural incorporation of heavy metal within Fe minerals (Nguyen et al., 2017). Although heavy metals were detected in the isolated, crystalline minerals by digestion, suggesting that the heavy metals were incorporated into the mineral structure, no significant XRD peak shift was discernable in this study. This most likely resulted from the relatively small amount of structural incorporation as well as the broadened peak shape (Fig. 1, Table 1).

Based on Mössbauer spectra, the fresh mineral products synthesized under Fe only and Na-bearing conditions contained two broad and symmetrical sextets representing magnetite, a relatively sharp sextet representing goethite, and a doublet (Fig. 2A, B and C). The Mössbauer spectra of the mineral precipitates under low-Cu condition and low- and high-Cd conditions were similar to those of Fe only and Na-bearing conditions (Fig. 2D, F and G). In contrast, Mössbauer spectra of the mineral precipitates under high-Cu condition and low- and high-Pb conditions only contained a relatively sharp sextet for goethite and a doublet, while the magnetite sextets disappeared (Fig. 2E, H and I). Therefore, Mössbauer analysis on these samples indicated consistent results with both XRD and MS. The doublet in ^{57}Fe Mössbauer spectrum typically represents superparamagnetism due to isomorphic substitution above 15 mol% and/or the size of mineral particles on the order of nanometers (Alvarez et al., 2015). Because this doublet was observed in

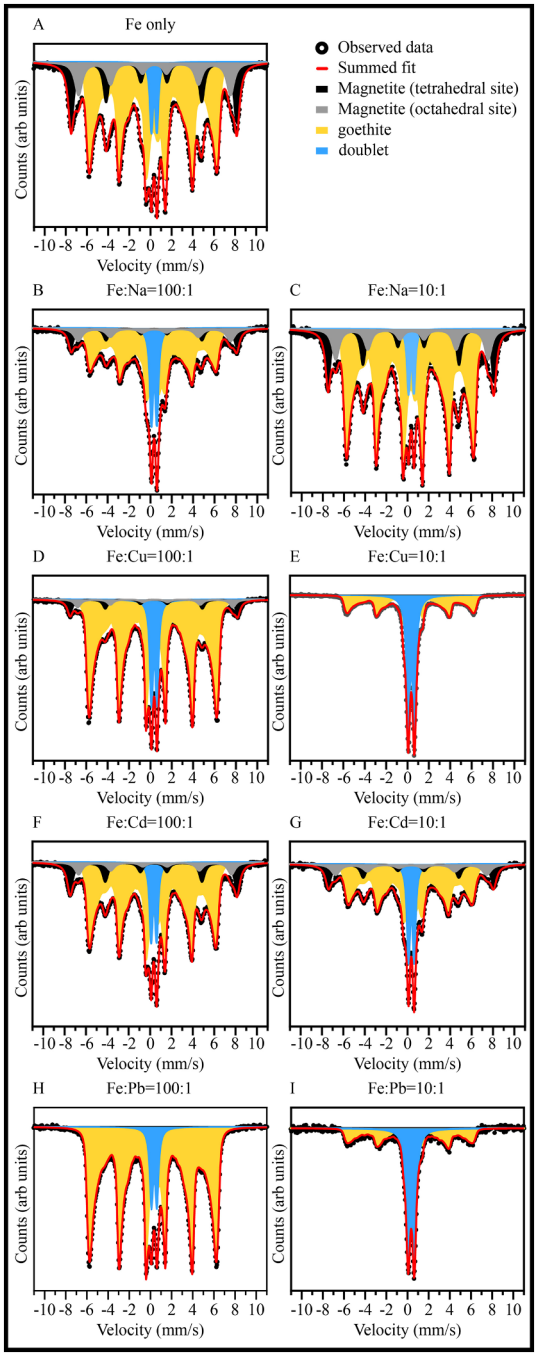

Fig. 2. Mössbauer spectra of the fresh Fe mineral products synthesized under different conditions. The red lines are the total calculated fits, through the black discrete data points. The resolved spectral components and assignments are tetrahedral Fe in magnetite (black area), octahedral Fe in magnetite (gray area), goethite (yellow area) and doublet (blue area).

all the mineral precipitates that were synthesized in this study (Fig. 2), it most likely originated from short-range-ordered nano-scale Fe(III) oxyhydroxide such as ferrihydrite and nanocrystalline goethite (nano-goethite). Based on Mössbauer spectra fitting, the minerals synthesized under Fe only, Na- and Cd-bearing conditions had a broadly similar composition, containing 20–31% of A_{mag}, 64–72% of A_{goe} and 5–15% of A_{dou} (Table 2). As for Cu- and Pb-bearing conditions, while the minerals synthesized under low-Cu condition still had 9 ± 2% A_{mag}, no magnetite could be detected in the samples that were synthesized under the other conditions. Additionally, the fractions of A_{dou}, i.e., ferrihydrite and/or nano-goethite, increased with higher concentrations of Cu and

Table 2
Mössbauer Fe assignments in the fresh Fe mineral products. Each Fe mineral (site population) was quantified by the spectral fitting as a fraction of the total Fe spectral area. Subscripts mag, goe and dou represent magnetite, goethite and doublet (ferrihydrite and/or nano-goethite), respectively. Results are reported in mole fractions (%) of total Fe. Results and uncertainties are calculated by MossWinn (Klencsar et al., 1996), and uncertainties are within 2% for each Fe mineral.

Synthesis condition	A_{mag} *(%)*	A_{goe} *(%)*	A_{dou} *(%)*
	Magnetite	*Goethite*	*Ferrihydrite and/or nano-goethite*
Fe only	31	64	5
Fe:Na = 100:1	21	66	13
Fe:Na = 10:1	27	69	5
Fe:Cu = 100:1	9	80	11
Fe:Cu = 10:1	0	49	51
Fe:Cd = 100:1	20	72	8
Fe:Cd = 10:1	24	61	15
Fe:Pb = 100:1	0	91	9
Fe:Pb = 10:1	0	45	55

Pb used during mineral synthesis. Furthermore, previous studies showed that changes in hyperfine magnetic field distribution of Fe minerals could indicate the incorporation of additional metal cations into the structure (Alvarez et al., 2015). While the hyperfine magnetic field distributions of the mineral precipitates that were synthesized under Fe:Me = 100:1 conditions appeared to be almost identical to those under Fe only condition, the distributions under Fe:Me = 10:1 conditions increased indeed in the low magnetic field, providing another line of evidence for structural incorporation (Fig. S1E, G and I).

As observed by high-magnification SEM (Fig. 3), the fresh mineral precipitates synthesized under Fe only and Na-bearing conditions contained ~10 nm ultrafine spherical particles as well as ~100 nm acicular and flaky particles. The SEM images of fresh minerals synthesized under low-Cu or Cd-bearing conditions looked similar to those obtained under Fe only and Na-bearing conditions. In contrast, the fresh mineral products synthesized under high-Cu condition and Pb-bearing conditions only contained acicular particles, while ultrafine spherical particles were not observed. The SEM images of the isolated, crystalline samples did not show any significant morphological difference compared to those of the corresponding fresh samples (Fig. 3 vs Fig. S2). Accordingly, although the isolation steps lowered the SSAs of most samples due to the removal of amorphous phases, the SSAs of the crystalline samples remained relatively high (Table 1). Corresponding to their mineral identity obtained collectively from XRD, Mössbauer and MS results, the spherical particle observed by SEM was most likely magnetite, and the acicular and flaky particle was most likely goethite. The particle sizes observed by SEM were also broadly consistent with the calculated XRD Scherrer widths (Fig. 3 vs Table S4). Furthermore, as indicated by SEM-EDS-mapping, the distributions of Fe and added heavy metals in the mineral precipitates were uniform (Fig. S3). The Fe:Me molar ratios (Me = Cu, Cd and Pb) were also calculated based on the compositional data from SEM-EDS, which agreed reasonably well with the bulk compositions derived from digestion (Table 1 vs Table S5).

3.3. Adsorption isotherms of resulting mineral products

Duplicate adsorption isotherms were performed to evaluate the sorption patterns of Cu, Cd and Pb on the crystalline mineral precipitates (Figs. 4 and S4). Adsorption experiments were not conducted on minerals synthesized under high-Pb condition because they, as already discussed earlier, dissolved completely during acid wash. The adsorption capacities of the resulting solids were proportional to the specific surface area (SSA) of the precipitates (Table 1 and Fig. S4). For example, the minerals synthesized under high-Cu conditions had a

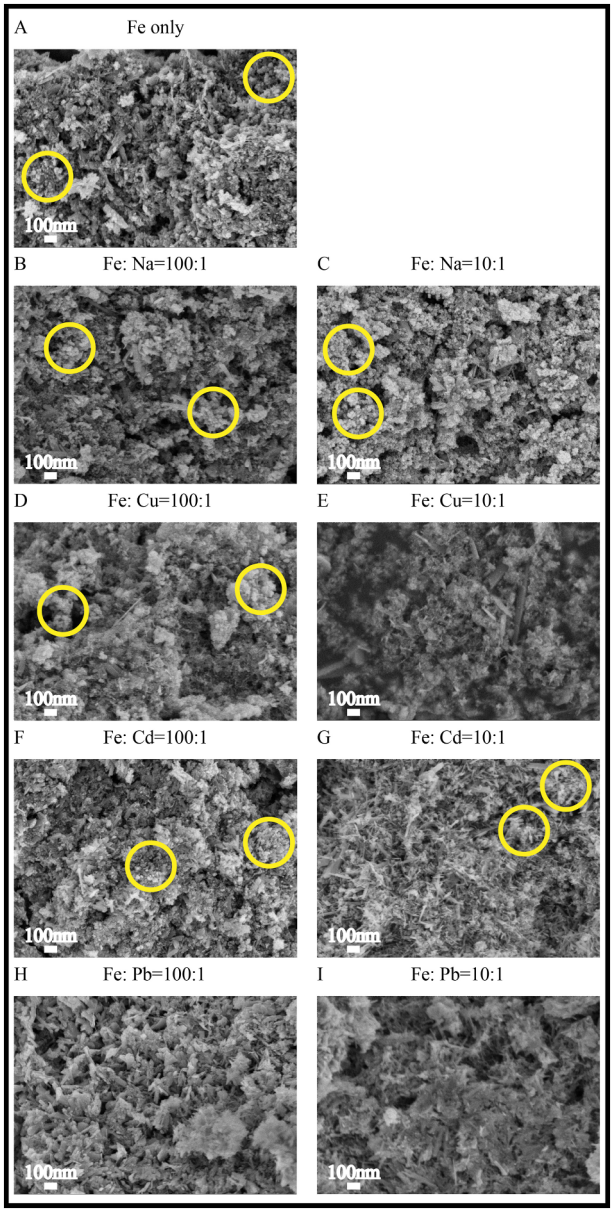

Fig. 3. SEM images of the fresh mineral products synthesized under different conditions. The ultrafine spherical particles were marked by yellow circles. The SEM images from the corresponding isolated, crystalline samples are shown in Fig. S2.

larger SSA and accordingly a larger adsorption capacity for Cu than the minerals under Fe only, Na-bearing and low-Cu conditions, respectively. Where the synthesized minerals possessed a similar SSA, they showed comparable amounts of sorbed Cu, Cd and Pb, respectively.

To isolate the effects of precipitate surface structure on heavy metal adsorption, all adsorption isotherms were normalized by the SSA (Fig. 4). Based on the SSA-normalized isotherms, the addition of divalent heavy metals during synthesis appeared to reduce the extent of heavy metal retention on the synthesized minerals. Generally, at pH 5.6, the adsorption capacity on the synthesized minerals followed the order Cu > Pb > Cd. For the added Cu concentrations, no clear asymptote in sorbed Cu concentrations was observed. The Pb isotherms were fitted with a Langmuir equation, resulting in adsorption maxima ranging between 1.44 and 2.33 μmol m^{-2}. The Cd isotherms showed consistently low adsorption, indicating that Cd had a low affinity for the synthesized minerals under the investigated experimental conditions. These observed adsorption patterns and capacities were consistent with the results of many previously reported studies on Cu, Cd and Pb adsorption on Fe oxide minerals, as summarized in Table S2.

4. Discussion

4.1. Mineral formation in the presence of different heavy metals

Based on their broad XRD peaks (Fig. 2), the high measured SSAs (Table 1) and the distributions in the low magnetic field in Mössbauer (Fig. S1), the precipitates formed during our magnetite synthesis showed to be poorly crystalline. As this was even the case for precipitates that were synthesized without additional heavy metals, we infer that the low crystallinity reflects the circumneutral pH of synthesis that was chosen to more closely mimic typical groundwater conditions (Faiyas et al., 2010; Jolivet et al., 2004; Schwertmann and Cornell, 2008). Amorphous ferrihydrite is often the kinetic product of Fe(III) hydrolysis (Schwertmann and Cornell, 2008; Zhu et al., 2016). Magnetite formation thus necessitates the conversion of ferrihydrite to magnetite (Hiemstra and van Riemsdijk, 2007). The first step in this recrystallization is the adsorption of Fe(II) to ferrihydrite. Ferrous Fe adsorption is, however, unfavorable under the conditions used in this study because the pH is lower than 7.6 ± 0.6, i.e., the pH_{zpc} (pH at the zero point of charge) of ferrihydrite (Kosmulski, 2009). At circumneutral pH, the ferrihydrite surface is positively charged, decreasing both the kinetics and the thermodynamics of cation adsorption, including Fe^{2+}. The suppression of Fe(II) adsorption prevents ferrihydrite recrystallization to more crystalline Fe oxides (Hiemstra and van Riemsdijk, 2007).

The second step in ferrihydrite recrystallization to magnetite or other crystalline minerals requires the electron transfer from adsorbed Fe(II) to structural Fe(III) (Hiemstra and van Riemsdijk, 2007). In this

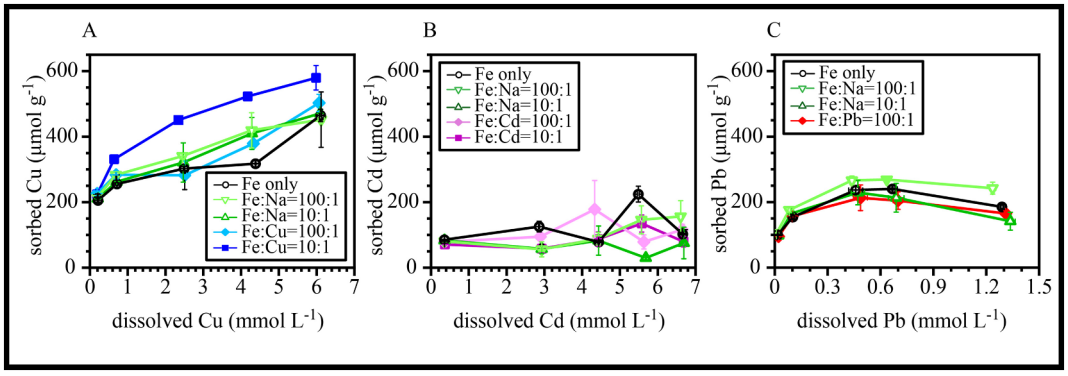

Fig. 4. Adsorption isotherms of (A) Cu, (B) Cd and (C) Pb on crystalline Fe mineral products synthesized under different conditions, which were normalized by the specific surface areas of the added minerals. Errors represent standard deviations between duplicate experiments, some of which are smaller than the size of symbols used.

study, in addition to circumneutral pH, coexisting heavy metal cations during synthesis led to structural substitution, further hindering the mineral growth of more crystalline Fe oxides. Previous studies have suggested that the presence of a redox-inactive divalent heavy metal within the lattice of Fe(III) minerals inhibits the electron transfer between adsorbed Fe(II) and structural Fe(III) (Latta et al., 2012). Accordingly, increasing additions of redox-inactive heavy metals present during synthesis resulted in the preservation of amorphous products like ferrihydrite rather than conversion to more crystalline precipitates (Table 2, Figs. 2 and S1).

Although magnetite formation was inhibited under the experimental conditions of this study, some magnetite was produced (Tables 1 and 2). The transformation of Fe(III) oxyhydroxides including ferrihydrite and goethite to magnetite relies on a relatively high surface loadings with Fe^{2+} (Hansel et al., 2005). As such, strongly adsorbing ions that decrease Fe^{2+} adsorption would significantly diminish magnetite formation. Our data suggest that the cations that were most effective at impeding magnetite synthesis (Pb^{2+}) adsorbed indeed much more strongly than the cations that only mildly (Cd^{2+}) or inconsequentially (Na^{+}) affected magnetite formation (Table 2, Figs. 2 and S1). Copper, which adsorbs to a similar extent as Pb^{2+} but more than Cd^{2+} at circumneutral pH, had a variable effect on magnetite formation, depending on the adsorption extent. In this study, XRD, Mössbauer and MS analyses consistently identified a small amount of magnetite being formed when sorbed Cu^{2+} concentrations were low (Fe:Cu ratio of 100), while no magnetite formed when sorbed Cu^{2+} concentrations were higher (Fe:Cu ratio of 10). Under circumneutral pH condition, Cu^{2+} has a higher affinity for mineral surfaces than Fe^{2+} (Liu et al., 2014; Vu et al., 2010). As a result, co-existence of Cu would reduce the surface loading of Fe(II) through competitive adsorption.

In this study, the divalent heavy metals (other than Fe) were added through nitrate-based chemicals. The oxidation of Fe(II) by the amended nitrate may have decreased the Fe(II) concentration and thus affected precipitate formation. This effect is usually minor because abiotic ferrous Fe oxidation by nitrate is slow (Gibney and Nusslein, 2007; Straub et al., 1996). However, while many divalent cations are not redox active themselves and do not catalyze Fe^{2+} oxidation by nitrate, this oxidation process can be catalyzed by dissolved Cu (Choi et al., 2012; Ottley et al., 1997). Thus, the presence of Cu^{2+} and nitrate would lead to the oxidization of Fe^{2+}, further suppressing magnetite formation. Different from Cu, the affinity of Cd^{2+} for mineral surfaces is lower than that of Fe^{2+} under circumneutral pH (Jeon et al., 2003), and the ability of Cd to catalyze the oxidation of Fe^{2+} by nitrate is negligible over the limited experimental time-scale of this study. Consequently, the mineral products from Cd-containing conditions were similar to those synthesized under Fe only condition (Table 2 and Fig. 1).

The effects of Pb^{2+} on magnetite formation are somewhat different because it is highly insoluble and thus forms mineral precipitates of its own. Lead is insoluble even at the low pH that prevailed before the pH of the system was elevated to initiate Fe mineral precipitation. This stems from the presence of sulfate counterions in the system and potentially also from carbonates that formed during CO_2 dissolution (Cadwalader et al., 2012). The calculated saturation indexes of amorphous $PbSO_4$ were 1.86 and 2.81 under low- and high-Pb conditions, respectively (Table S6). As a result, poorly crystalline $PbSO_4$ likely precipitated at least to some extent before Fe minerals formed (Kozawa et al., 2004). This $PbSO_4$ precipitate could have served as crystal nuclei of rapidly forming, poorly crystalline such as ferrihydrite (Sosso et al., 2016).

4.2. Ability to sequester heavy metals during and after mineral synthesis

The mineral products synthesized in the presence of additional heavy metals had widely variable compositions despite all of them being created from solutions of similar Fe:Me molar ratios (Table 1). Before isolation, the added heavy metals were sequestered in the fresh mineral products through direct mineral precipitation and/or (indirect) Fe mineral precipitation via structural substitution and/or sorption. In this study, independent of whether an initial ratio of Fe:Me = 100:1 or 10:1 was used, Cu and Pb were completely removed from solution during synthesis whereas only about half of the added Cd was removed (Table S3). Accordingly, the Fe:Cu and Fe:Pb ratios in the fresh mineral products were significantly smaller than the Fe:Cd ratio (Table 1). The smaller Fe:Cu and Fe:Pb ratios can be attributed to the higher affinities of Cu and Pb for the surface of Fe minerals (Fig. 4) and for Pb also the formation of $PbSO_4$ (Table S6). The isolation steps were unable to destroy stable, crystalline Fe minerals and the heavy metals that were incorporated within their structure (Sun et al., 2018a). However, they were able to remove adsorbed heavy metals, especially on amorphous high-SSA phases, as well as the $PbSO_4$ precipitate. Accordingly, while the Fe:Cd ratio did not change significantly between fresh and crystalline mineral products, the Fe:Cu and Fe:Pb ratios increased ~5 fold. Furthermore, while substitution of Cu and Cd within Fe minerals can take place (Cooper et al., 2006), due to the large difference in atomic radius between Pb and Fe, substitution of Pb within Fe minerals is expected to be less likely (Vu et al., 2010). However, in this study, the Fe mineral synthesized under low-Pb conditions contained Pb even after isolation, indicating a stable way for Pb sequestration, possibly associated with structural incorporation (Lu et al., 2020) or the adsorption on the defects of goethite (Vu et al., 2010).

Once formed, the ability of Fe minerals to sequester heavy metals relies primarily on surface adsorption. Although the adsorption isotherm experiment in this study was performed at mildly acidic pH instead of circumneutral pH, the results still allowed us to determine whether there is a difference in adsorption capacity between minerals synthesized with and without heavy metal additives. For Cd, the difference in adsorption capacity for Cd between the isolated, crystalline mineral precipitates synthesized under Cd-free and Cd-bearing conditions was subtle, at least partly due to the fact that Cd does not adsorb to Fe oxide minerals at acidic pH (Jiang et al., 2013). Nevertheless, based on the SSA-normalized adsorption isotherms (Fig. 4), the adsorption capacities of the Fe minerals synthesized under Cu- and Pb-bearing conditions decreased compared with their heavy metal-free analogues. This can be partially attributed to the increased pH_{zpc} of the minerals due to structural substitution of divalent heavy metal ions (Ni et al., 2017), preventing them from being conducive to the adsorption of positively charged heavy metals. Moreover, the adsorption capacity of the synthesized minerals increased with increasing magnetite content (Table 2, Fig. 4). This finding can be explained by the larger adsorption capacity of magnetite compared to goethite, which was the only other main mineral phase found in the crystalline samples. Various previous studies have demonstrated that the SSA-normalized adsorption capacity of magnetite for metal(loid)s is 3–4 times higher than that of goethite (e.g., Mamindy-Pajany et al., 2011; Uheida et al., 2006).

5. Conclusions

The motivation of this study was to assess the efficacy of in situ magnetite formation as a remediation strategy for heavy metal contaminated groundwaters. Our results clearly illustrate how magnetite formation and metal sequestration might be impacted by non-ideal, typical groundwater compositions, i.e., circumneutral pH conditions and the presence of a wider range of ions. Both of these factors seem to decrease the efficiency of magnetite formation, and the extent of metal incorporation in the resulting mineral products. At neutral pH, recrystallization was limited and, as a result, the Fe minerals formed were less crystalline, and frequently, not magnetite. The results also demonstrated that the presence of additional heavy metals during synthesis could affect the mineralogy and morphology of the Fe mineral products, which was regulated by the surface affinity of the heavy metal. The co-existence of heavy metal ions such as Cu and Pb during synthesis that have a higher affinity for mineral surfaces than Fe^{2+}

could suppress the surface loading of Fe(II) and thereby the mineral growth of more crystalline Fe oxides including magnetite. The surface affinity of the heavy metal would of course also regulate its adsorption capacity on the mineral products. Based on the SSA-normalized adsorption isotherms developed in this study, the incorporation of heavy metals in the mineral products noticeably lowered the extent of surface adsorption compared with their heavy metal-free analogues.

This study represents the first phase of the development of a magnetite-based remediation strategy for heavy metal cation contaminated groundwater, in which simplified experimental conditions were chosen in order to more clearly reveal the influence of coexistent divalent cations on the formation of magnetite. Continued efforts are clearly warranted for this magnetite-based method to eventually be used in real contaminated aquifers. The presence of many other solutes such as chloride, phosphate, carbonate and dissolved organic matter in real groundwater could impact heavy metal retention on minerals, by competing for surface sites, or by influencing mineral morphology and properties. The effects of individual solutes and their combinations clearly warrant further investigations. The applied synthesis procedure in this study produced relatively large fractions of Fe(III) oxyhydroxides under circumneutral pH conditions, which often have a high efficiency in removing heavy metal while being susceptible to subsequent redox changes that can occur in many heavy metal contaminated aquifers. Therefore, the composition of the amendments needs to be carefully refined such that a higher fraction of magnetite, the most suitable host-mineral for contaminant immobilization, can be created. One potential approach could be to add Fe(II) in multiple batches during the synthesis; by doing so, high dissolved and adsorbed Fe(II) concentrations could be maintained, thus stimulating a more sustained conversion of Fe(III) oxyhydroxides to magnetite. Identifying the optimal magnetite synthesizing procedure under environmentally relevant conditions is a focus of our ongoing research.

Declaration of competing interest

The authors declare no competing financial interest.

Acknowledgments

This study was financially supported by National Key Research and Development Program of China (No. 2019YFC1803600), National Natural Science Foundation of China (Nos. 41776188 and 41576183) and the National Institute of Environmental Health Sciences (Superfund Basic Research Program grant ES010349). Support for J.S. was provided partially by the Pioneer Hundred Talents Program of the Chinese Academy of Sciences. We would like to thank Y. Liang for his continuous support with the laboratory work. We also would like to thank Y. Fang, Z. Rao and J. Mou for their valuable input.

Appendix A. Supplementary data

Supplementary data to this article can be found online at https://doi.org/10.1016/j.chemgeo.2020.119669.

References

Adriano, D.C., Wenzel, W.W., Vangronsveld, J., Bolan, N.S., 2004. Role of assisted natural remediation in environmental cleanup. Geoderma 122 (2–4), 121–142.
Alvarez, M., Tufo, A.E., Zenobi, C., Ramos, C.P., Sileo, E.E., 2015. Chemical, structural and hyperfine characterization of goethites with simultaneous incorporation of manganese, cobalt and aluminum ions. Chem. Geol. 414, 16–27.
Cadwalader, G.O., et al., 2011. Erosion and physical transport via overland flow of arsenic and lead bound to silt-sized particles. Geomorphology 128, 85–91.
Choi, J., Batchelor, B., Won, C., Chung, J., 2012. Nitrate reduction by green rusts modified with trace metals. Chemosphere 86 (8), 860–865.
Coker, V.S., et al., 2006. XAS and XMCD evidence for species-dependent partitioning of arsenic during microbial reduction of ferrihydrite to magnetite. Environmental Science & Technology 40 (24), 7745–7750.
Cooper, D.C., Picardal, F., Rivera, J., Talbot, C., 2000. Zinc immobilization and magnetite formation via ferric oxide reduction by Shewanella putrefaciens 200. Environmental Science & Technology 34 (1), 100–106.
Cooper, D.C., Picardal, F.F., Coby, A.J., 2006. Interactions between microbial iron reduction and metal geochemistry: effect of redox cycling on transition metal speciation in iron bearing sediments. Environmental science & technology 40 (6), 1884–1891.
Crane, R.A., Scott, T.B., 2012. Nanoscale zero-valent iron: Future prospects for an emerging water treatment technology. J. Hazard. Mater. 211–212 (none), 112–125.
Delemos, J.L., Bostick, B.C., Renshaw, C.E., Sturup, S., Feng, X.H., 2006. Landfill-stimulated iron reduction and arsenic release at the Coakley Superfund Site (NH). Environmental Science & Technology 40 (1), 67–73.
EPA, U.S, 2013. Superfund Remedy Report, 14th edition. . https://clu-in.org/download/remed/asr/14/SRR_14th_2013Nov.pdf.
Faiyas, A.P.A., Vinod, E.M., Joseph, J., Ganesan, R., Pandey, R.K., 2010. Dependence of pH and surfactant effect in the synthesis of magnetite (Fe_3O_4) nanoparticles and its properties. J. Magn. Magn. Mater. 322 (4), 400–404.
Fu, R.B., et al., 2015. The removal of chromium (VI) and lead (II) from groundwater using sepiolite-supported nanoscale zero-valent iron (S-NZVI). Chemosphere 138, 726–734.
Ge, F., Li, M.M., Ye, H., Zhao, B.X., 2012. Effective removal of heavy metal ions Cd^{2+}, Zn^{2+}, Pb^{2+}, Cu^{2+} from aqueous solution by polymer-modified magnetic nanoparticles. J. Hazard. Mater. 211, 366–372.
Gibney, B.P., Nusslein, K., 2007. Arsenic sequestration by nitrate respiring microbial communities in urban lake sediments. Chemosphere 70 (2), 329–336.
Hansel, C.M., Benner, S.G., Fendorf, S., 2005. Competing Fe(II)-induced mineralization pathways of ferrihydrite. Environmental Science & Technology 39 (18), 7147–7153.
Hiemstra, T., van Riemsdijk, W.H., 2007. Adsorption and surface oxidation of Fe(II) on metal (hydr)oxides. Geochim. Cosmochim. Acta 71 (24), 5913–5933.
Jeon, B.H., Dempsey, B.A., Burgos, W.D., Royer, R.A., 2003. Sorption kinetics of Fe(II), Zn (II), Co(II), Ni(II), Cd(II), and Fe(II)/Me(II) onto hematite. Water Res. 37 (17), 4135–4142.
Jiang, W., et al., 2013. Arsenate and cadmium co-adsorption and co-precipitation on goethite. J. Hazard. Mater. 262, 55–63.
Jolivet, J.-P., Chanéac, C., Tronc, E., 2004. Iron oxide chemistry. From molecular clusters to extended solid networks. Chem. Commun. (5), 481–483.
Klencsar, Z., Kuzmann, E., Vertes, A., 1996. User-friendly software for Mossbauer spectrum analysis. Journal of Radioanalytical and Nuclear Chemistry-Articles 210 (1), 105–118.
Kosmulski, M., 2009. Compilation of PZC and IEP of sparingly soluble metal oxides and hydroxides from literature. Adv. Colloid Interf. Sci. 152 (1–2), 14–25.
Kozawa, A., et al., 2004. Basic understanding of the low current charge and high current charge for lead-acid batteries. Journal of Asian Electric Vehicles 2 (1), 577–578.
Latta, D.E., Bachman, J.E., Scherer, M.M., 2012. Fe electron transfer and atom exchange in goethite: Influence of Al-substitution and anion sorption. Environmental Science & Technology 46 (19), 10614–10623.
Liu, J., He, L.L., Dong, F.Q., Hudson-Edwards, K.A., 2016. The role of nano-sized manganese coatings on bone char in removing arsenic(V) from solution: Implications for permeable reactive barrier technologies. Chemosphere 153, 146–154.
Liu, T.X., Li, X.M., Waite, T.D., 2014. Depassivation of aged Fe0 by divalent cations: correlation between contaminant degradation and surface complexation constants. Environmental Science & Technology 48 (24), 14564–14571.
Liu, J., Luo, X., Sun, Y., Tsang, D., Qi, J., Zhang, W., Li, N., Yin, M., Wang, J., Lippold, H., Chen, Y., Sheng, G., 2019. Thallium pollution in China and removal technologies for waters: A review. Environ. Int. 126, 771–790.
Lu, Y., et al., 2020. Incorporation of Pb (II) into hematite during ferrihydrite transformation. Environmental Science: Nano 7 (3), 829–841.
Maher, B.A., 1988. Magnetic-properties of some synthetic sub-micron magnetites. Geophysical Journal-Oxford 94 (1), 83–96.
Mamindy-Pajany, Y., Hurel, C., Marmier, N., Romeo, M., 2011. Arsenic (V) adsorption from aqueous solution onto goethite, hematite, magnetite and zero-valent iron: Effects of pH, concentration and reversibility. Desalination 281, 93–99.
Muehe, E.M., et al., 2013. Organic Carbon and reducing Conditions Lead to Cadmium Immobilization by secondary Fe Mineral Formation in a pH-neutral Soil. Environmental Science & Technology 47 (23), 13430–13439.
Nassar, N.N., 2010. Rapid removal and recovery of Pb (II) from wastewater by magnetic nanoadsorbents. J. Hazard. Mater. 184 (1–3), 538–546.
Nguyen, X.S., Zhang, G.K., Yang, X.F., 2017. Mesocrystalline Zn-Doped Fe3O4 hollow submicrospheres: formation mechanism and enhanced photo-fenton catalytic performance. ACS Appl. Mater. Interfaces 9 (10), 8900–8909.
Ni, C.Y., Liu, S., Wang, H.L., Liu, H., Chen, R.F., 2017. Studies on adsorption characteristics of Al-free and Al-substituted goethite for heavy metal ion Cr (VI). Water Air and Soil Pollution 228 (1), 10.
Noubactep, C., Care, S., Crane, R.A., 2012. Nanoscale metallic iron for environmental remediation: prospects and limitations. Water Air and Soil Pollution 223 (3), 1363–1382.
Ottley, C.J., Davison, W., Edmunds, W.M., 1997. Chemical catalysis of nitrate reduction by iron (II). Geochim. Cosmochim. Acta 61 (9), 1819–1828.
Scherrer, P., 1918. Göttinger Nachrichten. Math. Phys 2, 98–100.
Schwertmann, U., Cornell, R.M., 2008. Iron Oxides in the Laboratory: Preparation and Characterization. John Wiley & Sons (22 pp).
Sorlini, S., Gialdini, F., 2010. Conventional oxidation treatments for the removal of arsenic with chlorine dioxide, hypochlorite, potassium permanganate and monochloramine. Water Res. 44 (19), 5653–5659.
Sosso, G.C., et al., 2016. Crystal nucleation in liquids: open questions and future challenges in molecular dynamics simulations. Chem. Rev. 116 (12), 7078–7116.
Statham, T.M., Stark, S.C., Snape, I., Stevens, G.W., Mumford, K.A., 2016. A permeable

reactive barrier (PRB) media sequence for the remediation of heavy metal and hydrocarbon contaminated water: a field assessment at Casey Station, Antarctica. Chemosphere 147, 368–375.
Straub, K.L., Benz, M., Schink, B., Widdel, F., 1996. Anaerobic, nitrate-dependent microbial oxidation of ferrous iron. Appl. Environ. Microbiol. 62 (4), 1458–1460.
Sun, J., Chillrud, S.N., Mailloux, B.J., Bostick, B.C., 2016a. In situ magnetite formation and long-term arsenic immobilization under advective flow conditions. Environmental Science & Technology 50 (18), 10162–10171.
Sun, J., et al., 2016b. Enhanced and stabilized arsenic retention in microcosms through the microbial oxidation of ferrous iron by nitrate. Chemosphere 144, 1106–1115.
Sun, J., Quicksall, A.N., Chillrud, S.N., Mailloux, B.J., Bostick, B.C., 2016c. Arsenic mobilization from sediments in microcosms under sulfate reduction. Chemosphere 153, 254–261.
Sun, J., et al., 2018a. Arsenic mobilization from iron oxides in the presence of oxalic acid under hydrodynamic conditions. Chemosphere 212, 219–227.
Sun, J., et al., 2018b. Model-based analysis of arsenic immobilization via iron mineral transformation under advective flows. Environmental Science & Technology 52 (16), 9243–9253.
Uheida, A., Salazar-Alvarez, G., Bjorkman, E., Yu, Z., Muhammed, M., 2006. Fe_3O_4 and gamma-Fe2O3 nanoparticles for the adsorption of Co^{2+} from aqueous solution. J. Colloid Interface Sci. 298 (2), 501–507.
Vu, H.P., Shaw, S., Brinza, L., Benning, L.G., 2010. Crystallization of hematite (alpha-Fe_2O_3) under alkaline condition: the effects of Pb. Cryst. Growth Des. 10 (4), 1544–1551.
Wang, J., Jiang, Y., Sun, J., She, J., Yin, M., Fang, F., Xiao, T., Song, G., Liu, J., 2020a. Geochemical transfer of cadmium in river sediments near a lead-zinc smelter. Ecotoxicol. Environ. Saf. 196, 110529.
Wang, J., Zhou, Y., Dong, X., Yin, M., Tsang, D., Sun, J., Liu, J., Song, G., Liu, Y., 2020b. Temporal sedimentary record of thallium pollution in an urban lake: An emerging thallium pollution source from copper metallurgy. Chemosphere 242, 125172.
Zhu, M., et al., 2016. Precipitation pathways for ferrihydrite formation in acidic solutions. Geochim. Cosmochim. Acta 172, 247–264.